A. Kumar¹*, B. Patham², S. Mohanty³, S. K. Nayak¹

Simulation-Based Approach for Probing Rheology-Processing-Structure Relationships in Foam Blow Molding

The broad objective of this work was to demonstrate a modelling and simulation framework for foam blow molding using commercially available simulation software. The simulation framework would have to account for the initial morphology of the foam, the relationship between the morphology and the rheological and deformation characteristics of the foam at high temperatures and high strains that are typically encountered during blow molding, and correlate the strains developed during blow molding to the morphological aspects in the resulting blow molded part. These aspects are addressed in this paper using simulations of uniaxial tensile deformation of a virtual representative volume element of a foam microstructure (rendered in DIGIMAT-FE) to derive the nonlinear tensile response of the foam at high temperatures (using ABA-QUS). The resulting simulated stress-strain curve is employed to parameterize a nonlinear rheological constitutive equation. These parameters are then employed for the homogenized representation of the foam in the blow molding simulation carried out in B-SIM, a commercially available simulation software for blow molding. The regions where the simulated parison has undergone primarily uniaxial elongation are then mapped back to the expected local foam morphology using the transfer functions derived from the RVE simulations. These steps result in a preliminary and simple demonstration of the simulation framework, and offer a template that can be detailed further with experimental rheological information on actual foamed parisons, and more detailed post-processing algorithms to correlate multiaxial elongations with microstructure.

1 Introduction

Polymeric foams are a very attractive class of materials due to their high specific stiffness and strength and their superior ther-

E-mail: anish83007@yahoo.com; anish.kumar@sabic.com

mo-mechano-acoustic isolation properties. Foams are widely employed in a variety of segments ranging from automotive, aerospace, appliances and packaging (American Chemistry Council Inc., 2015; Degischer and Kriszt, 2002; Eaves, 2004; Mills, 2007; Smith, 2015). From a processing perspective, extrusion and autoclave-based technologies for production of foam blocks, sheets and films are well established. These technologies have also been widely researched to probe the fundamental underpinnings of processing-structure-property interrelationships in such foams.

In the area of production of net-shaped parts, injection molding of course is a technology where foaming has made many inroads. Commercial injection molding machines already offer foaming technologies based on Mucell (Hayashi et al., 2010; MuCell Blow Molding, version 2017, MuCell Injection Molding, version 2017, Trexel, Wilmington, USA) and ProFoam (Gaub, 2017) and other customized molding technologies to cater to foaming, such as the core-back method (Miyamoto et al., 2015; Ruiz et al., 2016; Wu et al., 2018; Yusa et al., 2017).

However, more recently, the use of foaming in non-injection molding processes for production of net-shaped complex parts is gaining wider attention. These developments are both motivated by an increased amount of sophisticated needs emerging from various segments such as automotive and packaging, and also enabled by the availability of better process-control and instrumentation technology for foaming. From a technology perspective, foaming technologies such as ProFoam and Mucell are more mature and readily available to be incorporated as an overlaid operation to modify various existing extrusion and forming processes. From a segment perspective, for example, in the case of packaging – both rigid and flexible – foaming is the most attractive and readily available technology to make greater gains and push the boundaries in terms of downgaging and light-weighting of packages without compromise of the mechanical performance. Similarly, in automotive applications, while light-weighting through foaming is of obvious importance, the OEMs are also seeking multi-functionality in automotive parts thereby increasing single-material and sustainable solutions through foaming. For example, in under the hood applications for hot air ducts, foaming offers both light-

¹Central Institute of Plastics Engineering and Technology (CIPET), Chennai, India

²SABIC Technology Centre, Bangalore, India

³ Laboratory for Advanced Research in Polymeric Materials (LARPM-CIPET), Bhubaneswar, India

^{*} Mail address: Anish Kumar, Central Institute of Plastics Engineering and Technology, T. V. K. Industrial Estate, Guindy, Chennai, 600032, India

weighting, mechanical/vibrational damping, as well as thermo-acoustic isolation properties. Therefore, the use of foaming as an overlaid operation in production of net-shaped complex parts in non-injection molding processes such as blow molding (Mark et al., 2017; Peinado et al., 2015; Trexel, 2017a), thermoforming (Akkerman and Pronk, 1999), and multi-layer film extrusion (Sun and Liang, 2016) is being increasingly leveraged.

1.1 Motivation

As is the case with most emerging and state of the art processing technologies, the development of fundamental body of research providing insights and understanding on processing – structure - property relationships lags the actual empirical and commercial development of applications and instrumentation for foam blow molding. The situation for example, in the case of blow molding and thermoforming of foams may be contrasted with that of injection molded foams. Injection molding of foams is of course a relatively more mature technology, but more importantly, the fundamental understanding of the process and the simulation capabilities for injection foaming (e.g, foaming modules of commercially available simulation packages for injection molding such as AutodeskMoldFlow, version 2017, Moldflow, San Rafael, CA, USA and Moldex3D, version 2017, CoreTech System Co. Ltd., Chupei City, Hsinchu County Taiwan, ROC) have also caught up with the progress on application development in the recent years.

By contrast, thermoforming and blow molding of foams are relatively new technologies which have only in recent times found wider applications in both rigid packaging (e.g., shampoo bottles, yoghurt cups) and automotive (e.g., air ducts) (Smith, 2015; Trexel, 2017a). More importantly, the modelling and simulation methodologies and frameworks for such processes are still a research area in its infancy. Simulation frameworks for blow molding and thermoforming, even without

foaming are relatively recent developments. Commercial tools such as B-SIM (computer simulation of blow molding and sleeve shrinkage, version 2016, Accuform, Zlin-Stipa, Czech Republic) and BloView (version 2017, RheoWare Simulation Inc., Montreal, QC, Canada) for blow molding and T-SIM (computer simulation of thermoforming, version 2016, Accuform) for thermoforming are only recently gaining wider traction in an industry where product development and process optimization have been driven primarily by empirical trial-anderror and experience and skill. The overlaying of foaming in such simulation methods therefore remains quite an important but unaddressed need.

1.2 Foam Blow Molding Process Phenomenology

The processing of foam in extrusion blow molding is quite a challenging task (Zhu et al., 2007), as the foam has a two-phase microstructure that is subjected to high-strain deformation at high temperatures (in the vicinity of the melting point of the polymer) and at high strain rates. The phenomenology and the various processing-structure considerations in a typical extrusion foam blow molding processing set-up are summarized schematically in Fig. 1.

The foam blow molding process starts with the extrusion of a foamed parison, and this step includes phenomenological aspects such as the thermodynamics and kinetics of nucleation and cell growth, and the effect of the extrusion conditions, the die shape and the die land geometry on the foaming and the spatial distribution of foam density and cell size.

Further, the foamed parison can sag under gravity and therefore there can be further structure development of the foam under the influence of gravity before blowing happens. The foamed microstructure itself may in turn impact the sag behavior of the parison.

The parison is then inflated using pressurized gas to take the shape of the mold. During this step, in addition to the high-

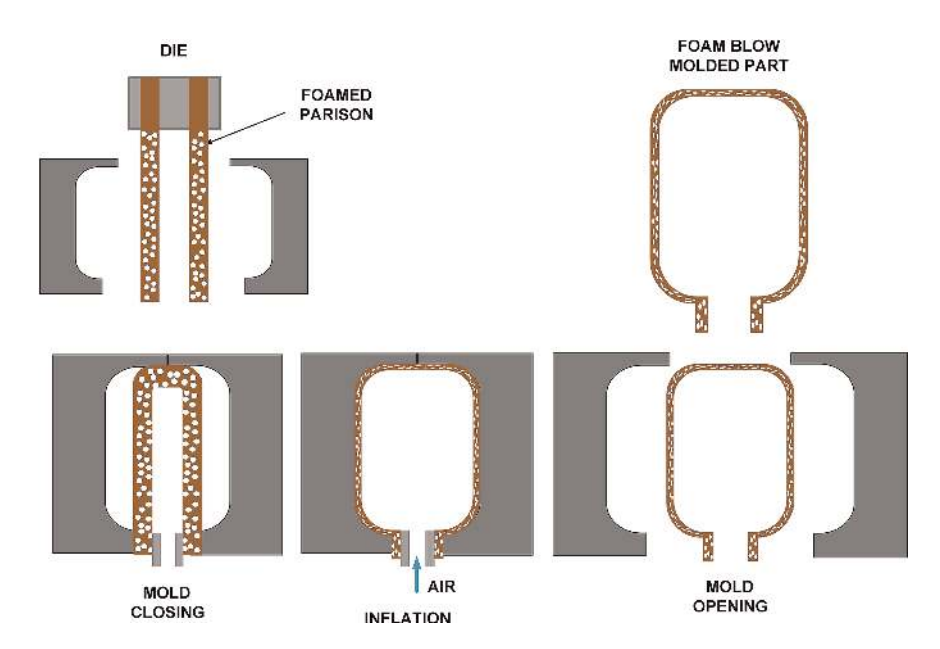


Fig. 1. Schematic showing various stages of foam blow molding, envisioning the anticipated foam microstructure evolution during blowing

strain deformation of the polymeric melt, a significant evolution of the foam structure is anticipated. During such deformations of the foam as encountered in blow molding, there are many possibilities in terms of stable or unstable morphology evolution at high strains (typically logarithmic strains of order of 1 beyond which significant strain hardening or extensional instabilities may be observed in many polymers). Some of the possibilities are schematically illustrated in Fig. 2.

For example, there may be skin formation on the mold-wall side and air blow sidewall, which may be desirable in most scenarios. This will also depend on the mold temperature and other conditions of processing. During the eventuality of unstable structure evolution, the foam voids may collapse at high temperatures and in the worst case, the foam structure may be completely lost. At high blowing pressures, cells on the edges may collapse which will restrict the formation of a continuous skin. The high temperatures may have an impact on the pressure inside the bubbles, leading to undesired evolution of foam microstructure. Further, during stretching of the parison, the foam structure will undergo not-insignificant deformation, which will further change foam morphology.

These unique challenges – driven by a close interrelationship between the morphology and processability and properties of the foamed product – require a specific simulation strategy for foam blow molding.

1.3 Scope

Therefore, the overall motivation of this research is to come up with a modelling and simulation framework for thermoforming or blow molding of foamed structures. The aim is to be able to make these modelling and simulation approaches compatible with commercially available software that simulate blow molding or thermoforming.

In terms of addressing the various stages of the phenomenology (cf. Section 1.2) using simulations, it is understood that the extrusion of foams and the effect of die and die land on the

foam production is a widely researched topic. Several equations of state are available to understand the nucleation and foam growth behavior and several simulation strategies are under development or investigation to understand the foam structure evolution due to pressure drop through the die flow. Simulation of parison sag remains a relatively unexplored problem, but that is not the primary focus of this report.

It also needs to be understood that commercially available software for blow molding such as B-SIM assumes a parison structure a priori and imposes the blow molding boundary conditions on this parison. Therefore, it may be argued that the parison itself, post-sag, forms the initial condition for the blow molding simulation. Therefore, in terms of taking the relevant piece of problem for further investigation, the scope of the framework development reported herein is focused on the downstream structure development of the foam during the blowing stage. The microstructure of the foam in the parison itself will be taken for granted, as it can be empirically measured or simulated using existing methodologies discussed in the foregoing. The blowing of the foamed parison will be the specific simulation focus addressed in this report.

1.4 Objectives

The key objective of carrying out a blow molding simulation of a foamed parison, the microstructure of which is known a priori, is to be able to successfully not only model the evolution of the macrostructure (thickness and strains within the blown part) but also to understand the foam microstructure changes during the process of blowing.

This objective may be broken down into two parts. The first part is to understand whether the high-strain behavior of foamed materials at temperatures in the vicinity of glass transition or melting point may be accurately captured using the material model that is available to simulate the material behavior during blow-molding in the commercial simulation software. The second part is to understand the insights one may derive

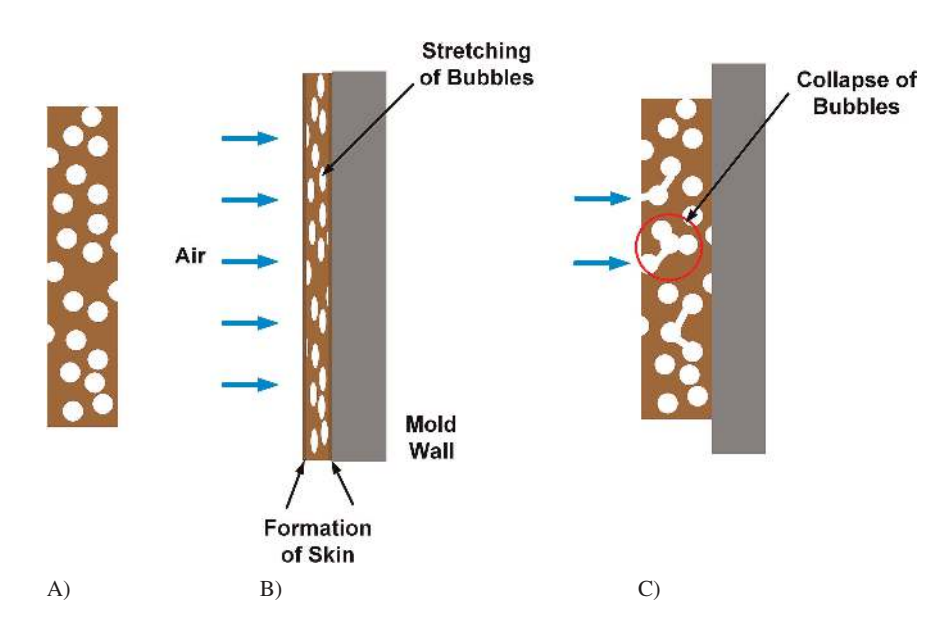


Fig. 2. Schematic showing the possibilities of foam morphology evolution during foam extrusion blow molding: A) extruded foam morphology in the foamed parison, B) stretching of the parison during blowing associated with extension of the cells and formation of skin and C) unstable foam morphology that may be associated with high extensional strains during blowing, leading to cell-collapse/coalescence

from a blow molding simulation into the correlations between the high-strain deformation during blow molding and the morphology evolution associated with such deformation history.

In addressing the first part objective it needs to be noted that commercially available software such as B-SIM does not account for multi-phase or multi-layer parisons. Therefore, a homogenized representation of the foam needs to be employed to represent the foamed parison. Further these tools widely employ nonlinear viscoelastic rheological constitutive models, particularly the integral Kaye Bernstein-Kearsley-Zapas (K-BKZ) (Bernstein et al., 1963; Tanner, 1988) constitutive equation, to address the highly nonlinear deformation associated with biaxial stretch during blow molding. Therefore, the key objective in terms of material modelling is to verify whether the K-BKZ model can present a realistic homogenized representation of the high-strain deformation of the foam at high temperatures. The blow molding simulation then would employ this homogenized model to simulate the thickness distribution in a blown part.

The second part objective of the framework then may be further focused on mapping back the local strains simulated by the blow molding simulation to the foam morphology. Of course, the aim in the long term (and not within the scope of the present study) would be to be able to gain insights into limiting processing conditions and limiting strains during blow molding which lead to undesired morphological/microstructural changes within the foam thereby setting a process-window for the foam blow molding process.

2 Approach

The various steps of the modelling and simulation approach detailed in the subsequent are summarized in Fig. 3, and are detailed in Sections 3 and 4.

Since the simulation approach starts with the foamed parison, the first step of the approach is to quantify the initial morphology of the foamed parison. Starting from this initial morphology, one needs to derive the homogenized representation of the high-strain deformation of the foam and model it using

the K-BKZ constitutive model. An important aspect of developing the rheological analysis is also to establish a transfer function between the stress-strain behavior of the foam with the morphological evolution.

It should be noted that developing a material model for homogenized representation of the foamed parison using experimental characterization would be quite involved. It would have required to take an actual foamed parison, freeze it so as to retain the initial microstructure, and then characterize the foam extracted from the parison under high-strain uniaxial and/or biaxial tensile deformation at high temperatures. The characterization would not only require the recording of the stress-strain behavior of the foam so as to parameterize the K-BKZ model, but also to track the evolution of the morphology of the foam with strain. This would either require sophisticated in-line optical measurements or freezing of the foam specimens at different strains and microscopy of the frozen specimens. This would then give us detailed morphology-rheology correlations. These steps are in progress with an actual foam and will be reported in a subsequent paper.

However, as mentioned earlier, the focus of this paper is mainly to evaluate whether simulation using a commercial blow molding software can indeed give us insights about foam blow molding. To address this specific goal, the elaborate experimental aspects associated with characterization of the viscoelasticity and microstructure-evolution of the foam were eschewed in favour of the use of a virtual representation of the foam microstructure. The stress-strain behavior of the foam then is derived (instead of laborious measurements) using a simulation of controlled load-case deformation of a representative volume element (RVE) of the foam microstructure, henceforth simply referred as RVE.

As shown in Fig. 3, the approach then would require the rendering of the RVE for representing the foam microstructure with realistic microstructural dimensional parameters. The creation of RVE was carried out in DIGIMAT FE (Digimat FE 2017 Documentation, MSC Software Corporation, Newport Beach, CA, USA), and is described in Section 3.1.2, and the various considerations in arriving at the RVE are detailed in the Appendix A2.

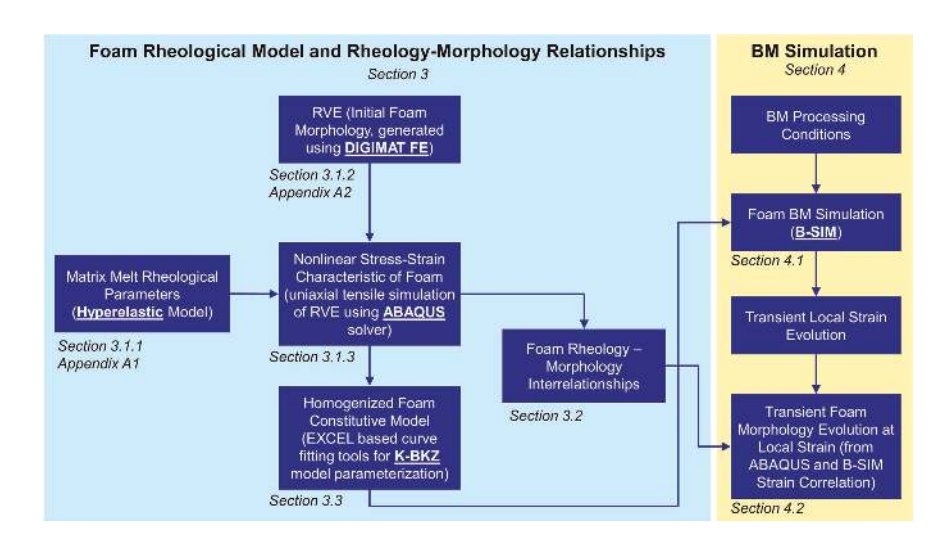


Fig. 3. Schematic delineating the steps of the approach, the software employed for the various steps and the sections within this article that describe the steps

The next step was to derive the nonlinear stress-strain response of the foam using a tensile deformation simulation of the RVE, with the assignment of realistic matrix properties to the matrix portions of the foam. The stress-strain response of the RVE was carried out in SIMULIA ABAOUS, version 2017, (Dassault Systems, Velizy-Villacoublay, France). In the ABAQUS simulation, the matrix material was assumed to be Hyperelastic and the strain-rate dependent characteristics of the matrix melt were not accounted for. Clearly, this is a simplistic representation of the matrix, and has been adopted for the sake of demonstration of the overall simulation framework of blow molding. A more realistic representation of the matrix is being employed in developing the material model for experimentally characterized foam systems, and this will be described in a subsequent report. In Section 3.1.1, the hyperelastic model parameters for the unfoamed melt, which also forms the matrix phase of the RVE are described. The considerations underlying the assignment of a material model for the matrix within the RVE, as well as details of the constitutive model are delineated in Appendix A1. The simulation of the tensile deformation of the RVE to obtain the stress-strain response of the foam is described in Section 3.1.3.

The RVE tensile deformation simulation also provides information about the evolution of the foam morphology, and the resulting morphology maps are presented in Section 3.2. After obtaining the stress-strain characteristic of the RVE using the ABAQUS simulation, the curve was analysed using the K-BKZ melt constitutive equation to obtain the relaxation spectrum and the damping function parameters corresponding to a homogenized representation of the foam. These aspects are described in Section 3.3.

The K-BKZ material model parameters for the foam can then be employed to carry out the blow molding simulation that provides information on the macroscopic deformation and strains in the resulting blow molded part. As mentioned before, the blow molding simulations were carried out using B-SIM (version 2.5, Accuform) for a model bottle geometry, and this is described in Section 4.1. The macroscopic strains estimated during blow molding using the B-SIM simulation were finally correlated with the foam morphology maps derived in Section 3.2 to assess the microstructure of the foam in the blow molded part. These aspects are described in Section 4.2.

3 Implementation of the Simulation Framework, Part I: Derivation of Rheological Parameters for Homogenized Representation of Foam

- 3.1 Derivation of Foam Nonlinear Stress-Strain Characteristics Using RVE Simulation
- 3.1.1 Assignment of Matrix Material Model for Foam RVE Properties of the Unfoamed Melt

For assigning the material properties to the matrix (the unfoamed melt) portion of the RVE, the rheological data for a widely characterized LDPE grade – studied in detail rheologically by Meissner (1971), and constitutively parameterized by Wagner (1976) and Chang and Lodge (1972) were chosen. The rheological characteristics of this strain-hardening melt

are summarized in Appendix A1. For representing the matrix phase in the RVE simulations that were carried out in ABA-QUS, instead of using a detailed nonlinear viscoelastic constitutive model for the unfoamed melt, a simpler 3-mode Ogden hyperelastic model was chosen. The motivations underlying the use of the hyperelastic model, as well as the parameterization of the Ogden model using the experimental data from Wagner are also described in Appendix A1. The resulting Ogden model parameters for the unfoamed melt at 150 °C are listed in Table 1. Additionally, the Poisson's ratio was taken as 0.475 (ABAQUS, Analysis User's Guide, version 2016, Dessault Systems) i.e. nearly incompressible material.

In Fig. 4, the experimentally measured extensional stress growth data at 1 s⁻¹ from Meissner (converted into engineering stress-strain) are compared with the estimates from ABAQUS tensile simulations using the 3-mode Ogden hyperelastic model. As can be seen, the match is adequate.

| N | μ _i Pa | $lpha_{ m i}$ | | |
|---|----------------------|---------------|--|--|
| 1 | 715.813 | 3.7603 | | |
| 2 | -369.475 | 3.9685 | | |
| 3 | 33 311.620 | -3.4034 | | |

Table 1. Ogden material constants employed for the unfoamed melt representing the matrix phase in the foam RVE (based on extensional stress growth data for LDPE melt at 150°C studied by Meissner (1971); see Appendix A1)

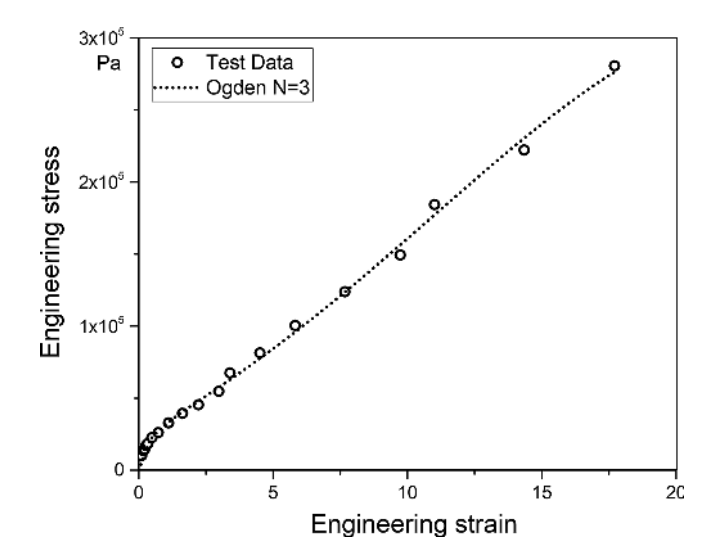


Fig. 4. Extensional stress growth characteristic of the unfoamed melt modelled using an elastomer material model: The experimental extensional stress growth data for LDPE melt from Meissner (Meissner, 1971; Wagner, 1976) at $1 \, s^{-1}$ (converted into engineering stress-strain) is compared with estimated stress-strain curves using a multi-element ABAQUS simulation with assignment of the Ogden N=3 material model for the matrix

3.1.2 Definition of the RVE

The considerations underlying the choice and design of the RVE are described in the Appendix A2. As described in Appendix A2, a detailed parametric study was carried out on a number of RVEs to represent foams. In the parametric study, each RVE, with a chosen setting of the parameters such as the RVE size, cell number density, cell size and cell size distribution within the RVE was generated in DIGIMAT. The stress-strain response of the RVE – with the polymer matrix melt modelled as hyperelastic as described in Section 3.1.1 – under uniaxial extension at constant true strain rate was then simulated using ABAQUS.

The uniaxial tensile deformation simulation setup, along with a grid independence study that was also carried out to select an appropriate mesh size to carry out the simulations, is also described in Appendix A2.

It was clear from this parametric study that at a given cell volume fraction (representing a constant relative density of the foam) the parameters such as the RVE size, cell number density, cell size and cell size distribution within the RVE had minimal or no impact on the predicted uniaxial tensile stressstrain response of the RVE. From these studies the cell volume fraction emerged as the key parameter governing the magnitudes of stresses generated by the foam. This parameter was then taken forward for investigation by generating four RVEs with cell volume fractions ranging from 0.2 to 0.5, as shown in Fig. 5. Based on the conclusions of the parametric study, the RVEs were designed so as to achieve quick simulation turnaround times by employing a small RVE size. It may be seen from Fig. 5 that to achieve higher cell volume fractions of 0.4 and 0.5, imposing a cell size distribution was required, while the RVEs with the lower volume fractions were generated with more uniformly sized cells.

3.1.3 Stress-Strain Characteristics of the Foam RVE – Effect of Cell Volume Fraction

The stress-strain curves estimated from ABAQUS simulations of uniaxial tensile deformation of the four RVEs shown in

Fig. 5 at a constant true strain rate $1~\rm s^{-1}$, using the 3-mode Ogden model representation for the matrix, are plotted in Fig. 6 (please refer to Appendix A2 for description of the relevant boundary conditions). The nominal (engineering) stress was computed by the ratio between the simulated reaction force on the top face and the initial cross section area of the RVE.

Along with the estimated curves for the foam, the stress-strain response for the unfoamed melt is also plotted for reference (the data for the unfoamed melt is the same as the data plotted in Fig. 4, but in Fig. 6, the engineering stress in plotted against true strain instead of engineering strain).

Note: For the RVE simulations in ABAQUS, only the momentum balance was solved for. No thermal energy balance was carried out; in other words, the simulations represent isothermal conditions for the foam deformation, and as such no inputs regarding the RVE temperature were provided. However, it may be noted that since the hyperelastic material parameters

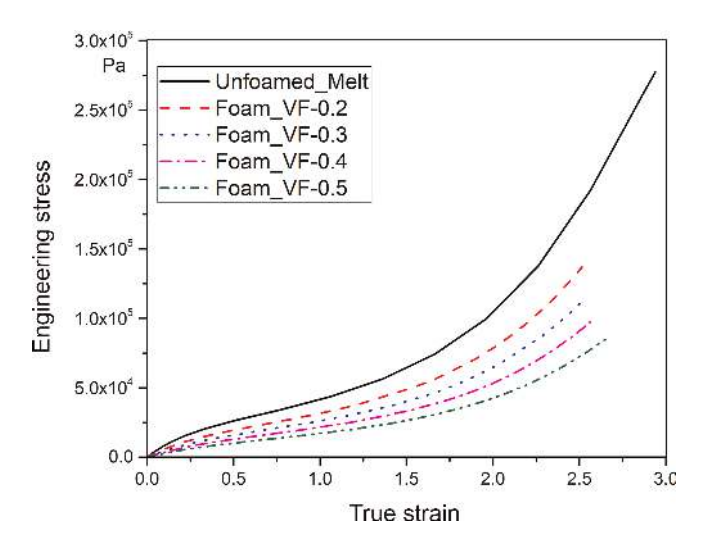


Fig. 6. Estimated uniaxial tensile stress-strain curves at true constant extensional strain rate of $1\ s^{-1}$ for the four RVEs representing foams with different cell volume fractions, simulated using ABAQUS (with the matrix property simulated using the Ogden model with parameters shown in Table 1)

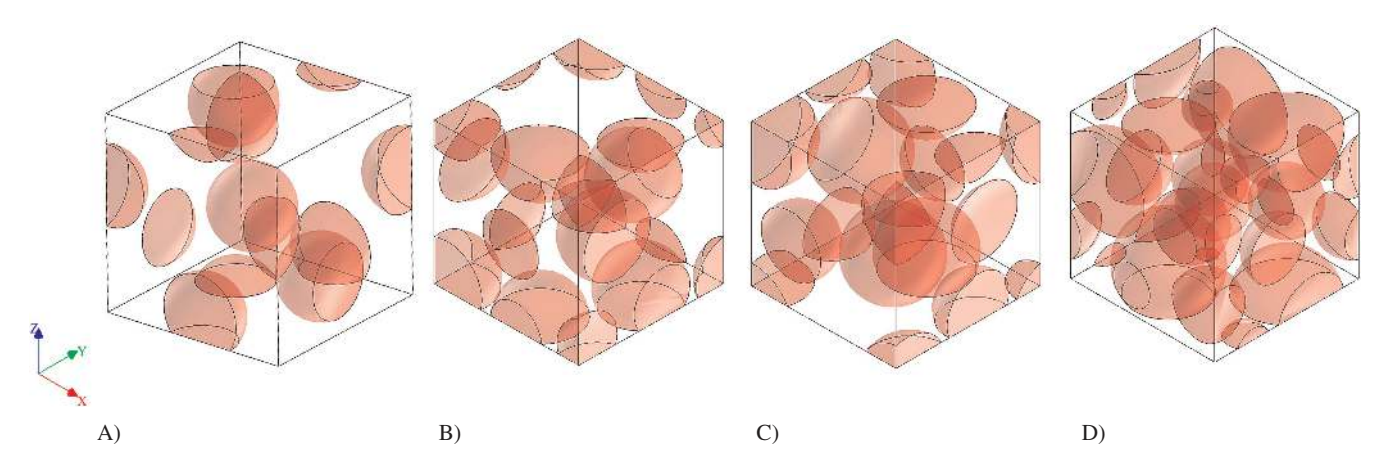


Fig. 5. RVEs for representing foams with cell volume fractions A) 0.2, B) 0.3, C) 0.4, and D) 0.5. All the four RVEs have been created with the same total RVE volume

for the matrix correspond to experimental data for the LDPE melt at $150\,^{\circ}$ C, all the RVE simulations effectively represent foam deformation at $150\,^{\circ}$ C.

From Fig. 6, it may be noted that the foams also display strain hardening behavior at true strains of 1 and above; this is consistent with the strain hardening behavior of the unfoamed melt, accurately captured by the hyperelastic material model. It can be seen that the estimated curves for the foam RVEs lie below that of the unfoamed melt, as expected. The magnitudes of the stresses for the foams at comparable strains progressively decrease compared to the unfoamed matrix with increase in the cell volume fraction. The reduction in stresses, quantified as the ratio of stress estimated for the foam to that of the unfoamed melt, is listed for different magnitudes of true strains in Table 2.

From Table 2, it is clear that for a given cell volume fraction, the stress ratios remain more or less constant over the entire range of strains; an average of the stress ratios at the different strains is recorded as a "Scale Factor", and this will be discussed further in the context of the K-BKZ constitutive model parameterization in Section 3.3. It is interesting to note that for all the foams, the stress ratios are similar to, but slightly lower than the assigned cell volume fraction of the corresponding RVE.

The stress strain curves estimated from the RVEs are very valuable because they now represent homogenized material properties for the foams as a whole. The stress-strain curves, and the underlying simulations, contain strong imprints of the foam morphology evolution with increasing uniaxial strain, thus providing important information on the morphology-rheology interrelations for the foams.

3.2 Derivation of Foam Morphology Evolution Characteristics Using RVE Simulation

Figure 7 shows the morphologies predicted at different strains along the uniaxial extension curve for the foams. As can be seen from Fig. 7, at true strain of about 1.5, significant exten-

sion in the voids and the development of significant proximity between adjacent voids may be observed.

Further analysis of local stresses within the matrix around the voids revealed that around the same strains, stress concentrations occur close to the vertices of the elongated voids, indicating significant plastic deformation within the matrix in these regions. These are also the regions where the matrix may fail under tensile stresses, leading to cell collapse or coalescence. However, in the RVE simulation, no failure criteria for the matrix were used, therefore no inference about cell collapse or coalescence may be made. Of course, it can be understood that by simple extension of the simulation to incorporate matrix failure criteria, cell collapse and coalescence may also be modelled through an analogous simulation. Therefore, the morphology map presented in Fig. 7, while a little simplistic, still points to the potential insights that may be obtained from RVE simulations in understanding the foam behavior during large extensional deformations.

3.3 Foam K-BKZ Constitutive Parameters

The commercially available software for blow molding, B-SIM, that we employed for this study employs the K-BKZ constitutive equation (Bernstein et al., 1963; Tanner, 1988) for the polymeric melt. The stress-strain curves for the foam RVE were modelled using the K-BKZ model to obtain the constitutive parameters for the blow molding simulations in B-SIM, as described hereunder. The K-BKZ model is a fully nonlinear viscoelastic constitutive model that accounts for both the time-dependence using a memory function, and strain-dependence using a strain damping function as shown in Eq. 1 below.

$$\underline{\underline{\sigma}}(t) = \int_{-\infty}^{t} \mu^{0}(t - t') h\{I_{1}(t, t'), I_{2}(t, t')\} \underline{\underline{C_{t}^{-1}}}(t') dt'. \tag{1}$$

The memory function describes the linear viscoelastic (purely time dependent) behavior, governed by the reptation characteristics of the polymeric melt (Ferry, 1980), that is given as shown:

| Strain | Simulated stress Pa | | | | Stress ratio | | | | |
|------------------|------------------------|----------|----------|----------|--|----------------------|----------|----------|----------|
| Unfoamed melt | | Foam | | | Stress in foam/Stress in unfoamed melt | | | | |
| | ment | VF – 0.2 | VF – 0.3 | VF – 0.4 | VF – 0.5 | VF – 0.2 | VF – 0.3 | VF – 0.4 | VF – 0.5 |
| 0.5 | 26131 | 19539 | 15 891 | 12937 | 10 186 | 0.75 | 0.61 | 0.50 | 0.39 |
| 1 | 41 673 | 31519 | 26 247 | 21 596 | 17 181 | 0.76 | 0.63 | 0.52 | 0.41 |
| 1.5 | 64 572 | 48740 | 40 27 1 | 33 107 | 26485 | 0.75 | 0.62 | 0.51 | 0.41 |
| 2 | 104576 | 78517 | 64618 | 53310 | 42 580 | 0.75 | 0.62 | 0.51 | 0.41 |
| | | | | | | Average scale factor | | | |
| | | | | | | 0.75 | 0.62 | 0.51 | 0.40 |

Table 2. The estimated stresses from the RVE simulations at different strains for the foams with different void volume fractions, compared with the stresses at corresponding strains in the unfoamed melt, resulting in a scaling factor for the foam stress-strain curves

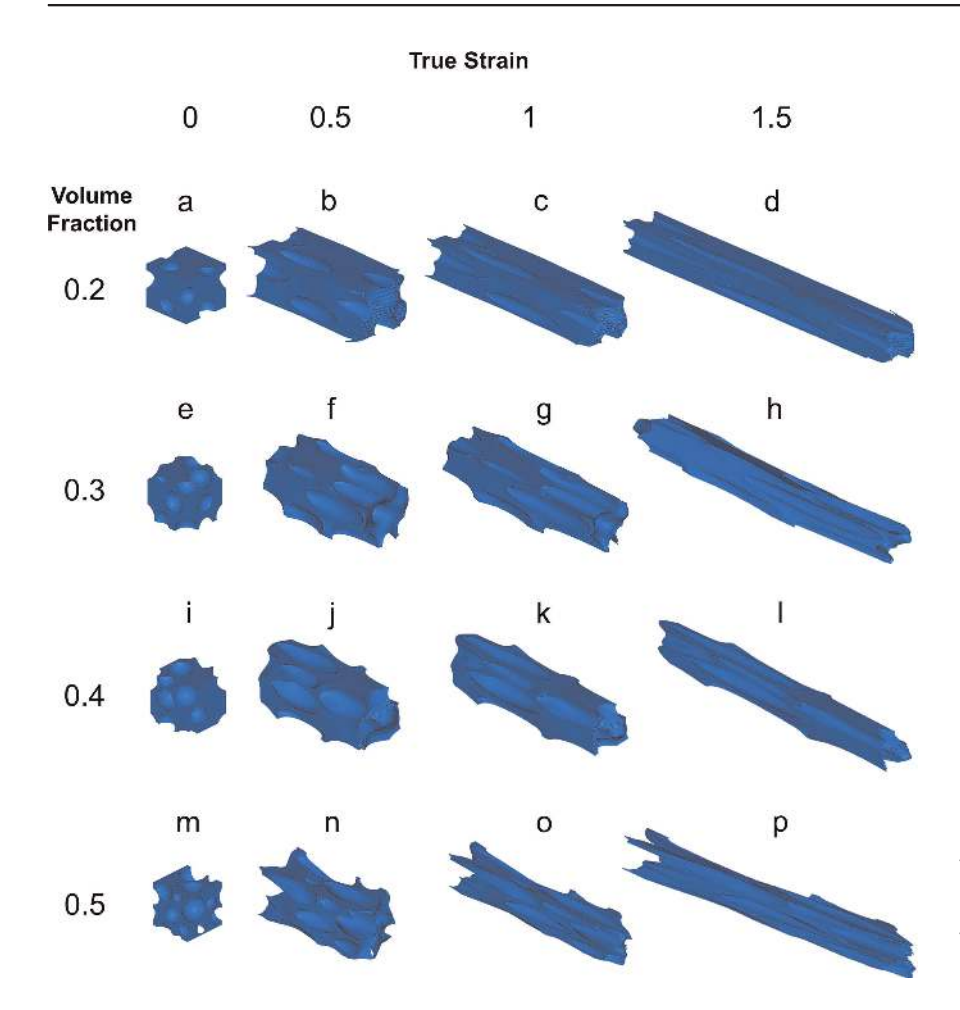


Fig. 7. The simulated foam RVE morphology evolution during uniaxial tensile deformation at true strains of 0, 0.5, 1.0, and 1.5, for the RVEs representing foams with cell volume fraction of 0.2 (a-d), 0.3 (e-h), 0.4 (i-l) and 0.5 (m-p); obtained from the ABAQUS uniaxial tensile deformation simulation for the foam RVE at a true constant extensional strain rate 1 s⁻¹ using the 3-mode Ogden model representation for the matrix

$$\mu^0(t-t') = \sum_i \frac{g_i}{\lambda_i} exp[-(t-t')/\lambda_i], \eqno(2)$$

where g_i and λ_i are the Prony series constants describing the viscoelastic stress relaxation behavior (cf. Equations A1 and A2 in Appendix A1). The strain dependent term, called the damping function (Ferry, 1980; Kasehagen and Macosko, 1998), can take the form as shown in Eq. 3 (cf. Wagner (Christopher, 1994; Wagner, 1976)).

$$h(I_1,I_2) = exp\Big[-(n-\delta)\sqrt{I_2-3} - \delta\sqrt{I_1-3}\Big], \eqno(3)$$

here, n and δ are arbitrary constants that are employed to fit the damping function to the high strain behavior.

For startup extensional stress growth experiment as simulated using the RVE, in which the uniaxial true strain (logarithmic or Hencky strain ϵ) is increased at a constant true extensional strain rate $\dot{\epsilon}$, the Finger strain takes the form shown below.

$$C_t^{-1}(t') = \begin{bmatrix} exp[2\dot{\epsilon}(t-t')] & 0 & 0 \\ 0 & exp[-\dot{\epsilon}(t-t')] & 0 \\ 0 & 0 & exp[-\dot{\epsilon}(t-t')] \end{bmatrix}, \label{eq:ct}$$

and therefore, the invariants of the Finger strain tensor are:

$$I_1 = \exp[2\dot{\epsilon}(t - t')] + 2\exp[-\dot{\epsilon}(t - t')], \tag{5}$$

$$I_2 = 2\exp[\dot{\varepsilon}(t - t')] + \exp[-2\dot{\varepsilon}(t - t')]. \tag{6}$$

Combining Eqs. 1 to 6, the extensional stress growth during start-up uniaxial extension at a constant extensional rate $\dot{\epsilon}$, may be expressed as

$$\begin{split} \sigma_{11}(t) - \sigma_{22}(t) &= \int\limits_{0}^{t} \sum_{i} \frac{g_{i}}{\lambda_{i}} exp[-(t-t')/\lambda_{i}] h\{I_{1}(t,t'),I_{2}(t,t')\} \\ \cdot &\{ exp[2\dot{\epsilon}(t-t')] - exp[-\dot{\epsilon}(t-t')] \} dt' + \{ exp[2\dot{\epsilon}t] \\ - &exp[-\dot{\epsilon}t] \} h\{I_{1}(t),I_{2}(t) \} G^{0}(t). \end{split} \tag{7}$$

Therefore, the full parameterization of the K-BKZ model then requires the determination of the viscoelastic Prony series constants g_i and λ_i and the damping function parameters n and δ .

It should be noted that due to the use of a virtual RVE for the foam, there were no direct insights available into the purely viscoelastic (linear time-dependent) behavior of the foam. The stress strain curve generated from the RVE simulation only presents a high strain deformation scenario for the foam. It does not, however, give any handles to capture the time-dependent or viscoelastic parameters.

Two possibilities were considered for generation of the relaxation spectrum. The first was to carry out the simulation with the foam RVE to mimic a dynamic mechanical loading test. This would entail a complex simulation setup and require detailed post-processing analysis to de-convolute the output stresses from the simulation to get the storage and loss moduli of the foam. The second possibility was to verify whether the relaxation spectrum of the unfoamed melt may be scaled systematically to obtain the spectrum for the foam. The latter option, which was simpler, was explored first, and resulted in a robust scaling strategy for shifting the relaxation spectra, as summarized below. The first option involving a dynamic simulation was therefore not explored further. The relaxation spectrum and the damping function constants which give the best fit with the RVE simulation data are shown in Table 3.

To obtain the relaxation moduli for the foams, the relaxation modulus of the unfoamed melt (same as that of the LDPE melt from the studies of Meissner (1971)) was multiplied by the estimated stress "Scale Factor" (obtained from the ratio of the simulated uniaxial stress of the foam and that of the unfoamed melt; cf. Table 2) corresponding to the respective volume fraction. With the scaled relaxation spectrum listed in Table 3 for each foam, an EXCEL based solver routine was then employed to calculate the K-BKZ uniaxial stress growth using Eq. 7, by iteratively varying the damping function parameters n and δ , to minimize the error between the RVE-simulated curve and the estimate of the K-BKZ equation. The K-BKZ estimates for uniaxial tensile stress growth for the foams with varying void volume fractions are overlaid on the simulated stressstrain response obtained using the corresponding RVEs in Fig. 8.

It can be seen that the K-BKZ model with the parameters listed in Table 3 performs adequately to predict the RVE-simulated uniaxial stress-strain behavior of the foams at all the volume fractions. It is very interesting to note that the stress scaling factor derived from the stress-strain curves for the foam

RVEs relative to that of the unfoamed melt provides a robust factor for scaling the relaxation moduli of the resulting foams. It should be noted that the stress scaling factor is similar to, and only slightly lower than, the volume fraction of the matrix for each foam. However, the use of the matrix volume fraction directly as the scaling factor to shift the relaxation moduli did not result the same quality of fits. The K-BKZ parameters listed in Table 3 were then employed for the blow molding simulation of the foamed parison as discussed in the next Section

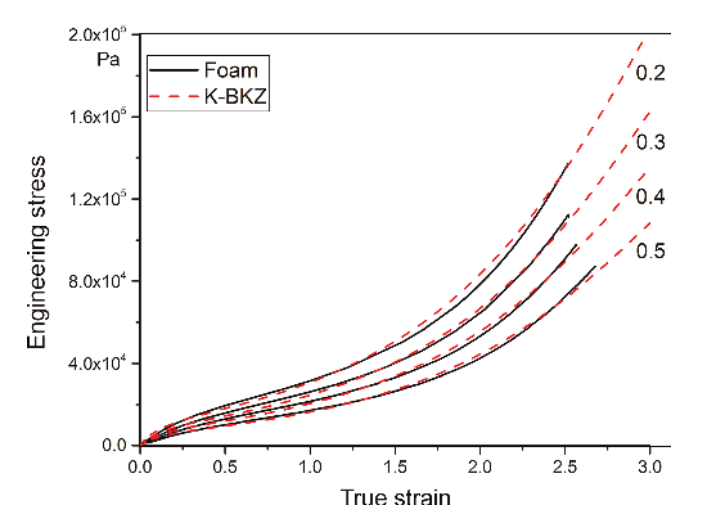


Fig. 8. K-BKZ estimate for different volume fractions (using the constants listed in Table 4) for uniaxial tensile stress growth for the homogenized rendition of the foam, compared with the simulated stress-strain response using the heterogeneous foam RVE

| i | Relaxation time s | Relaxation modulus Pa | | | | | |
|-----------------------------|-------------------------------|---|--|--|---|--|--|
| | | Unfoamed melt (Wagner, 1976) | VF – 0.2 | VF – 0.3 | VF – 0.4 | VF – 0.5 | |
| 1 2 3 4 5 | 100 10 1 0.1 0.01 | 190.3 2306 6241 32990 37200 | 142.72 1729.50 4680.75 24742.5 27900 | 117.98 1429.72 3869.42 20453.8 23064 | 97.05 1 176.06 3 182.91 16825 18972 | 76.12 922.40 2496.40 13 196.0 148 80.0 | |
| Damping function parameters | | Unfoamed melt (Wagner, 1976) | Foams | | | | |
| n δ | | 0.143 0.1 | 0.2 0.02 | | | | |

Table 3. Relaxation spectrum and damping function parameters for the foams derived by fitting of the simulated stress-strain curve of the RVE, and through scaling of the matrix relaxation spectrum

4 Implementation of the Simulation Framework, Part II: Blow Molding Simulation

4.1 B-SIM Simulation Setup

Blow molding simulations are demonstrated in the context of a simple geometry — a bottle with a circular cross-section (Fig. 9A for the dimensions and Fig. 9B for the blow mold cavity rendered in CAD). The extrusion blow molding step to achieve this geometry — starting from a circular cylindrical foamed parison — was simulated using B-SIM. The foamed parison was modelled as a single-phase material using the K-BKZ material model derived in the foregoing; in the subsequent, we present results for the parison assigned with the K-BKZ material parameters for the foam with void volume fraction of 0.2. The circular cylindrical parison was set up with a diameter of 34 mm, thickness 3 mm and 5000 mesh elements. The initial temperature of the parison was uniformly set to 150 °C.

The process control parameters in B-SIM include the inflation time, inflation pressure and the tool movement. The approximate inflation time and pressure can be determined as (Crawford, 1998):

$$t = \frac{\lambda B_{ST} h_d}{P D_d} \left\{ 1 - B_{ST}^2 \left(\frac{D_d}{D_m} \right) \right\}, \tag{8}$$

$$P = \frac{2h\sigma}{D_m}, \tag{9}$$

where λ is tensile viscosity, B_{ST} is swelling of parison diameter (D_1/D_d) , D_1 is parison diameter, D_d is die diameter, h_d is die thickness, P is inflation pressure, D_m is mold diameter, h is fi-

nal part thickness and σ is hoop stress. Using the above relationship, the total inflation time and blowing pressure were set to 1.5 s and 300 Pa respectively. The pressure setting is significantly lower compared to what would be required to blow an unfoamed matrix part; this is of course due to the lower tensile strength and viscosity of the foam material obtained from simulation, and also designed so as to prevent the bubbles to collapse in actual practice. The mold travel time was not considered and the process was assumed to start with the molds closed (post pinch-off).

The K-BKZ material model parameters for the homogenized representation of the foam (Table 3) derived as described in Section 3 were assigned to the parison material. The mold temperature was set at 40 °C. The heat transfer coefficients between the mold and material, and to the ambient were assigned default values ascribed within B-SIM. The friction coefficient between the mold and parison material was set at 0.5.

4.2 Analysis of B-SIM Simulation Output

The relative placements of the parison and the cavity for the B-SIM simulation, and the simulated blow-molded part are shown in Fig. 10. The distribution of the simulated thickness of the blow molded bottle along a longitudinal section (Fig. 11A) is plotted in Fig. 11B.

However, the evaluation of the precise strain distribution at each section within the simulated geometry is not straightforward from post-processing of B-SIM results due to the multi-axial extensions involved during the blowing of the parison. The deformation of the mesh associated with the blow molding

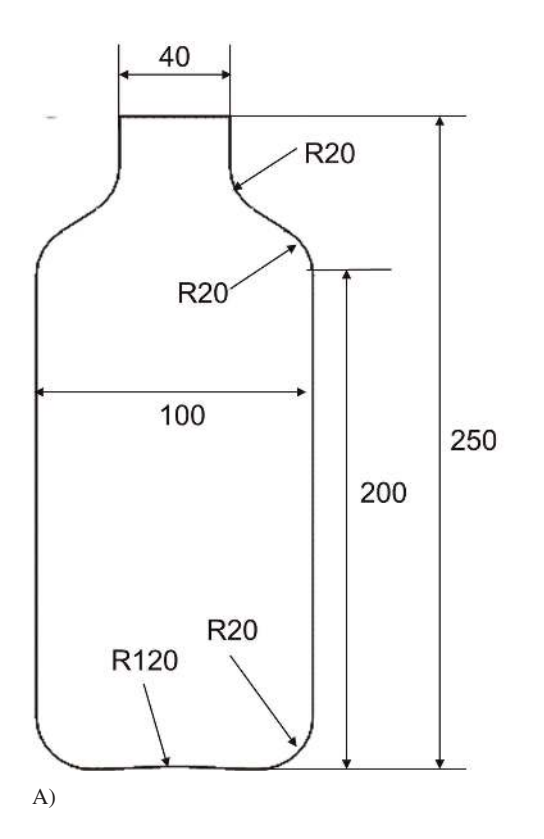




Fig. 9. Geometrical dimensions of a circular cross-section bottle (A) and CAD drawings of the associated symmetric blow molding cavity (B), employed in the B-SIM simulation trials

step can be visualized using the collage seen from the Fig. 12. A squared region consisting of four elements is considered from parison (Fig. 12A) and its deformation is traced to the final blown part (Fig. 12B). The impact of the expansion of the parison under the impact of blow-pressure at an elemental level is schematically shown in Fig. 12C, and the inferred deforma-

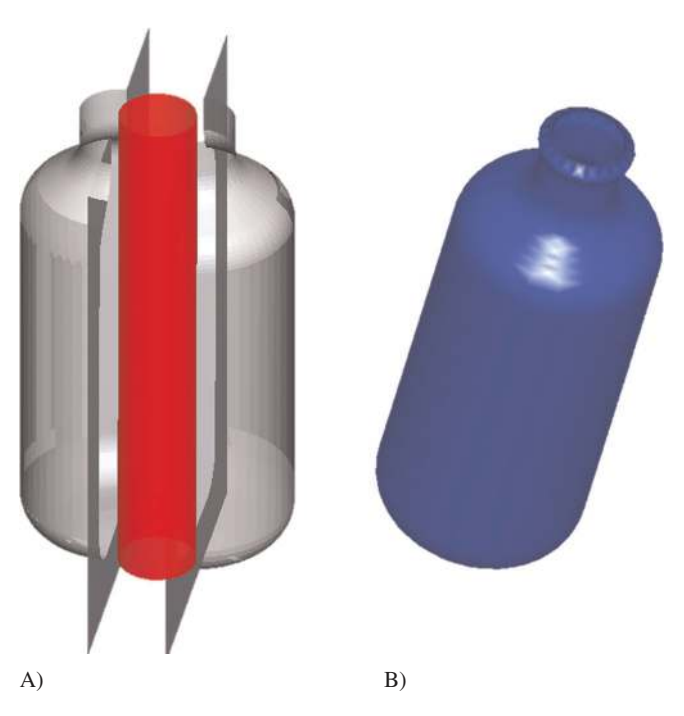


Fig. 10. Blow molded part: B-SIM images showing the pinch-off areas of the cavities relative to the parison (A) and the final blown part for a circular cross-section bottle (B)

tion of an ideal single void in the region is visualized in Fig. 12D. The aim of creating a strain-map is to then infer the corresponding deformation of the two-phase microstructure corresponding to the local strain.

From Fig. 12 it is clear that depending on the region within the part geometry where the element is located, it may undergo multi-axial deformation or even purely uniaxial deformation. Translating multi-axial deformation information into strain requires a more detailed post-processing analysis to derive the components of the associated local strain tensor. Further, it also requires the morphology map associated with multi-axial states of stress, which was not within the scope in the preliminary RVE analysis discussed in Section 3.

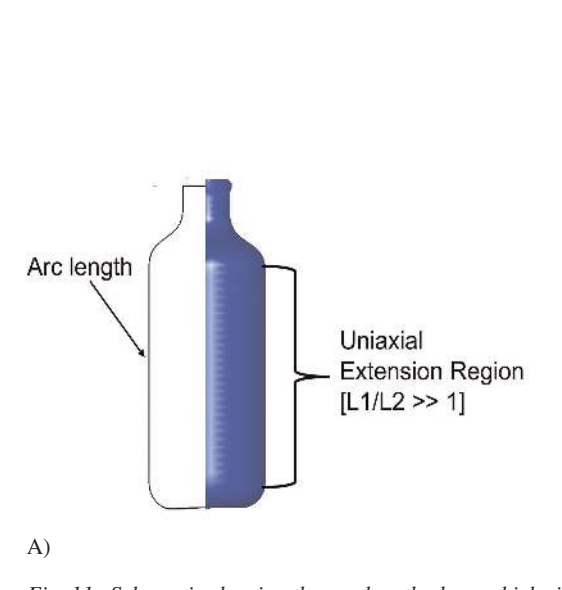
However, in regions where the extension is primarily uniaxial the strains may be unambiguously evaluated. Further, as discussed in Section 3, the foam morphology evolution under uniaxial tensile deformation was derived using the RVE simulation. Therefore, we will discuss the morphological transformations of foam only in the context of regions where the extensions are primarily uniaxial. The methodology to identify such regions and to obtain a morphology map is described briefly in the subsequent.

B-SIM simulation output can be employed to get a map of planar extensions along the blown part. The planar extension is defined as the average extension expressed in terms of extensions in principal directions (B-SIM V2.5 Reference – Blow molding simulation, version 2016, Accuform):

$$\varepsilon_{\text{Planar}} = \sqrt{\lambda_1 \lambda_2},$$
 (10)

where λ_1 and λ_2 are the extension ratios in two principal directions and expressed in terms of final length (l) and the initial length (L) as:

$$\lambda_1 = \frac{l_1}{L_1}, \lambda_2 = \frac{l_2}{L_2}. \tag{11}$$



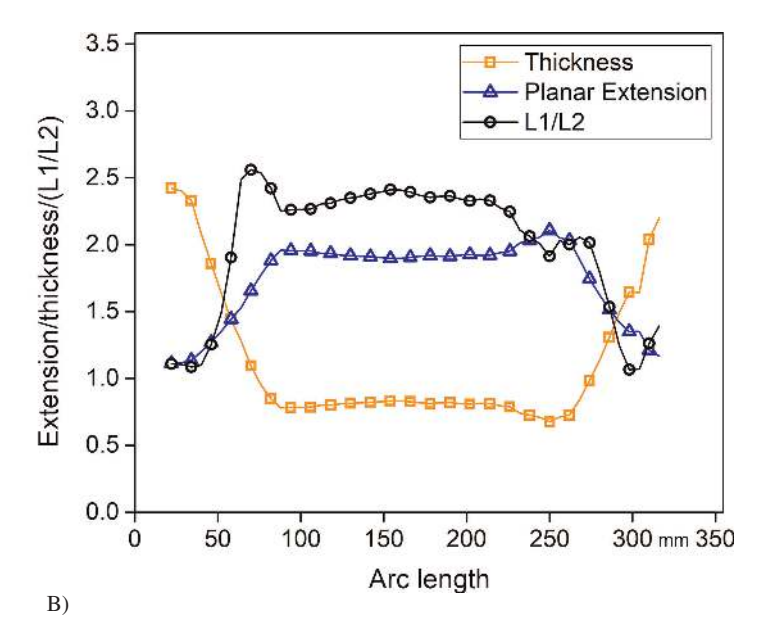


Fig. 11. Schematic showing the arc-length along which simulation outputs were measured, for the circular cross-section bottle (A), and the estimated thickness distribution, planar extension and the ratio of extensions in principal directions plotted along this arc (B)

From the simulation result, the ratio of relative extensions in two principal directions defines the uniaxial and biaxial deformations (B-SIM V2.5 Reference – Blow molding simulation, version 2016, Accuform).

If
$$\frac{L_1}{L_2} \gg 1$$
, deformation is almost uniaxial, (12)

If
$$\frac{L_1}{L_2} = 1$$
, deformation is equibiaxial. (13)

The planar extensions and the relative extension in the two-principal directions, extracted along the longitudinal cross-sectional arc (cf. Fig. 11A) of the circular bottle have also been plotted along with the thickness distribution in Fig. 11B. From an inspection of the magnitudes of the extension ratios, it may be seen that in the middle straight cylindrical region of the bottle the parison has undergone almost uniaxial deformation. On the other hand, the regions in the neck and the bottom of the bottle have a biaxial deformation and hence we are not considering these regions for the measurement of Hencky strain. The Hencky strain in uniaxial deformation region can be calculated as (B-SIM V2.5 Reference – Blow molding simulation, version 2016, Accuform)

$$\varepsilon = \ln\left(\sqrt{\lambda_1 \lambda_2}\right) \forall \frac{L_1}{L_2} \gg 1. \tag{14}$$

Figure 13 shows the expected foam morphology in the blow molded part in the regions where the parison has undergone predominantly uniaxial tensile deformation. This is the relatively straight cylindrical portion of the bottle (away from the bottom and the neck) where the cylindrical parison undergoes expansion in the radial direction leading to development of hoop strains resulting in Hencky strains ranging from 0.64 to 0.75. At these strains the cells inside do not show significant stretch, nor is any significant thinning of matrix bridges between the cells noticed.

Figure 13 is an example of the morphological information that may be derived from the blow molding simulation, thereby exemplifying the insights that may be derived from combining detailed foam rheological measurements with blow molding simulations.

5 Summary and Next Steps

A nonlinear viscoelastic integral constitutive model (K-BKZ + Wagner) has been developed for homogenized representation of the foam deformation at high temperatures and to high strains. A preliminary understanding of foam morphology evolution when subjected to large-strain uniaxial deformations at high temperatures has been gained through simulations with a virtual foam representative volume element. The homoge-

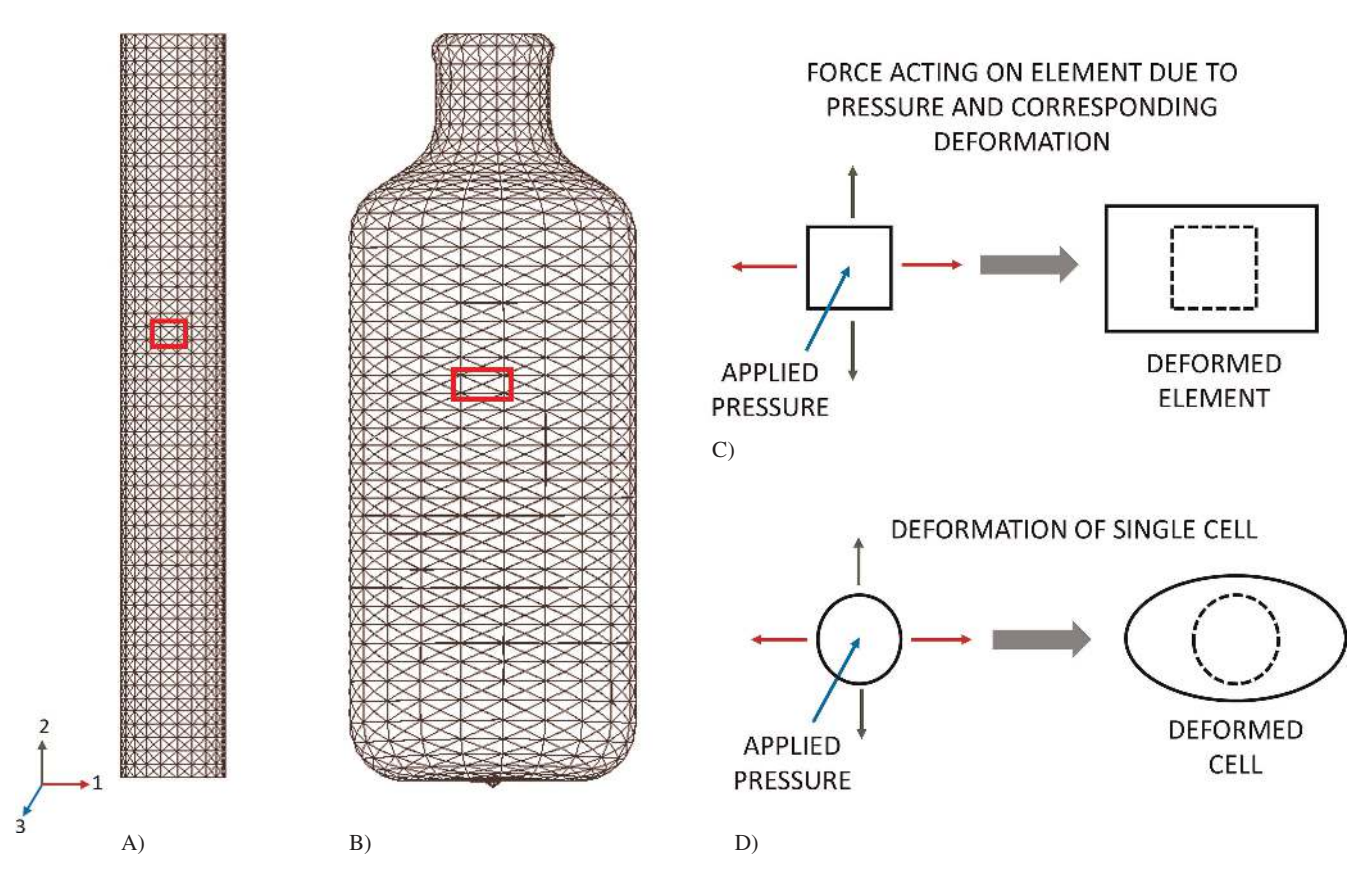


Fig. 12. Panel that traces an element from the parison (A) to the blown part (B), and further, explaining the strains encountered by (C) an element during blowing, and by (D) a foam cell during biaxial stretch during blowing

nized rheology model for foam has been parameterized and implemented on B-SIM simulation software. Regions with primarily uniaxial extension have then been mapped back to the state of foam morphology at corresponding Hencky strains. The next steps in making this framework more detailed are as follows.

From the perspective of the use of virtual RVE for deriving the foam rheological behavior, the next steps would be:

- To assess morphology development in more complex loading scenarios such as non-equi-biaxial and planar stretch, and to correlate the state of morphology to invariants of the strain tensor.
- In representing the matrix, accounting for viscoelastic (rate dependent) effects more accurately.
- Addressing morphology development in foams with high volume fraction of voids.
- Provisioning for cell coalescence and collapse through the use of appropriate damage propagation and failure criteria for the matrix.

From the perspective of the derivation of material model for the foam, the ongoing and future work emphasises on:

Experimental rheological characterization of real foams (in contrast to the virtual RVE) – first with relatively simple specimens such as sheets, and then with an actual foamed parison – and developing experimental protocols to parameterize the relaxation spectrum and high-strain damping function, combined with qualitative and quantitative assessment of morphology evolution. As in the case of studies with virtual RVEs, the experiments with real foams would also entail the correlation of foam extension and

morphology in more complex loading states (e.g., biaxial extension).

From the perspective of the use of commercial tools for simulation of foam blow molding, the key next step would be:

- Development of post-processing algorithms for tools such as B-SIM to obtain maps of equivalent strain measures and strain tensor invariants in regions where parison undergoes multi-axial extension during blowing, and subsequently, user-defined routines and visualization techniques to translate strain maps to foam morphology maps based on information provided by the users.
- Research and development on several of these aspects are in progress and will be detailed in subsequent reports.

References

Akkerman, R., Pronk, R., "Vacuum Forming of Thermoplastic Foam",
 Polym. Eng. Sci., 39, 2064–2074 (1999), DOI:10.1002/pen.11598
 American Chemistry Council Inc., "Polyurethane Applications",
 https://polyurethane.americanchemistry.com/Applications (2015)

Bardella, L., Sfreddo, A., Ventura, C., Porfiri, M. and Gupta, N., "A Critical Evaluation of Micromechanical Models for Syntactic Foams", Mech. Mater., **50**, 53–69 (2012), DOI:10.1016/j.mechmat.2012.02.008

Bernstein, B., Kearsley, E. A. and Zapas, L. J., "A Study of Stress Relaxation with Finite Strain", Transactions of the Society of Rheology, VII, 391–410 (1963), DOI:10.1122/1.548963

Bower, A. F.: Applied Mechanics of Solids, 1st Edition, CRC Press, Boca Raton (2010), DOI:10.1002/cbdv.200490137

Chang, H., Lodge, A. S., "Comparison of Rubberlike-Liquid Theory with Stress-Growth Data for Elongation of a Low-Density Branched

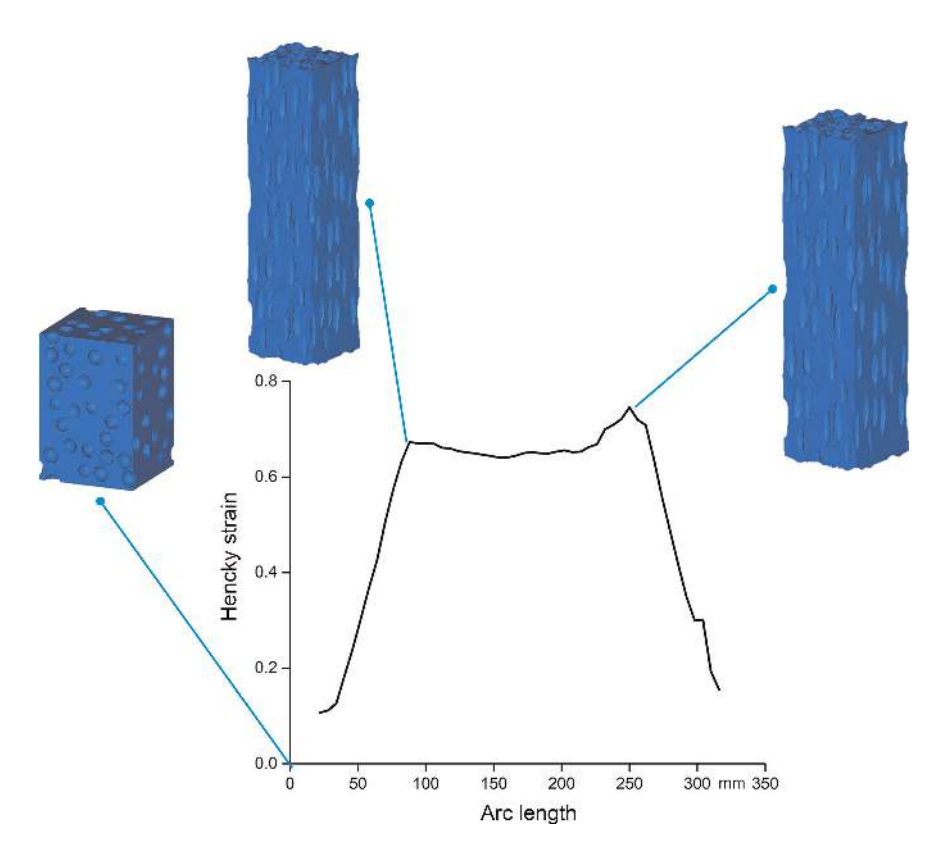


Fig. 13. Uniaxial extension along the arc of the circular cross section bottle (cf. Fig. 11A) mapped to the foam morphology

- Polyethylene Melt", Rheol. Acta, **11**, 127–129 (1972), DOI:10.1007/BF01992879
- Cho, Y., Lee, W. and Park, Y., "Finite Element Modeling of Tensile Deformation Behaviors of Iron Syntactic Foam with Hollow Glass Microspheres", Materials, 10, 1201 (2017), PMid:29048346; DOI:10.3390/ma10101201
- Christopher, W. M.: Rheology: Principles, Measurements, and Applications, 1st Edition, Wiley-VCH, New York (1994)
- Crawford, R. J.: Plastics Engineering, 3rd Edition, Butterworth-Heinemann, Oxford (1998), DOI:10.1016/B0-12-227410-5/00587-1
- Degischer, H. P., Kriszt, B.: Handbook of Cellular Metals Production, Processing, Applications, 1st Edition, Wiley-VCH, Weinheim (2002), DOI:10.1002/3527600558
- Eaves, D.: Handbook of Polymer Foams, 1st Edition, Rapra Technology Ltd., Shawbury (2004)
- Ferry, J. D.: Viscoelastic Properties of Polymers, 3rd Edition, John Wiley & Sons, New York (1980)
- Gaub, H., "Profoam Cost-Efficient Process for Manufacturing Foamed Lightweight Parts", Reinf. Plast., 61, 109–112 (2017), DOI:10.1016/j.repl.2015.12.074
- Hayashi, H., Mori, T., Okamoto, M., Yamasaki, S. and Hayami, H., "Polyethylene Ionomer-Based Nano-Composite Foams Prepared by a Batch Process and Mucell Injection Molding", Mater. Sci. Eng., **30**, 62–70 (2010), DOI:10.1016/j.msec.2009.08.009
- Kasehagen, L. J., Macosko, C. W., "Nonlinear Shear and Extensional Rheology of Long-Chain Randomly Branched Polybutadiene", J. Rheol., 42, 1303–1327 (1998), DOI:10.1122/1.550892
- Mark, L. H., Chu, R. K. M., Wang, G. L. and Park, C. B., "High-Pressure Preform Foam Blow Molding", Int. Polym. Proc., 32, 637–647 (2017), DOI:10.3139/217.3537
- Marur, P. R., "Numerical Estimation of Effective Elastic Moduli of Syntactic Foams", Finite Elem. Anal. Des., 46, 1001–1007 (2010), DOI:10.1016/j.finel.2010.07.006
- Meissner, V. J., "Dehnungsverhalten von Polyethylen-Schmelzen", Rheol. Acta, 10, 230–242 (1971), DOI:10.1007/BF02040447
- Mills, N. J.: Polymer Foams Handbook: Engineering and Biomechanics Applications and Design Guide, 1st Edition, Butterworth-Heinemann, Oxford (2007)
- Miyamoto, R., Utano, T. and Yasuhara, S., "Effect of Crystals and Fibrous Network Polymer Additives on Cellular Morphology of Microcellular Foams", in AIP Conference Proceedings 1664, 040001, pp. 1–4, (2015), DOI:10.1063/1.4918399
- Peinado, V., García, L., Fernández, Á. and Castell, P., "Lightweight Medium-Sized Parts Made of Foamed HDPE Processed via Extrusion Blow Moulding: Analysis of Parison Formation", Adv. Mech. Eng., 7, 1–12 (2015), DOI:10.1155/2014/681293
- Ruiz, J. A. R., Vincent, M. and Agassant, J.-F., "Numerical Modeling of Bubble Growth in Microcellular Polypropylene Produced in a Core-Back Injection Process Using Chemical Blowing Agents", Int. Polym. Proc., 31, 26–36 (2016), DOI:10.3139/217.3129
- Shahzad, M., Kamran, A., Siddiqui, M. Z. and Farhan, M., "Mechanical Characterization and FE Modelling of a Hyperelastic Material", Mater. Res., 18, 918–924 (2015), DOI:10.1590/1516-1439.320414
- Smith, D., "101 Applications for Expanded Polystyrene & Polypropylene", https://www.dssmith.com/foam-products/insights/101-applications-for-polystyrene (2015)
- Sun, X., Liang, W., "Cellular Structure Control and Sound Absorption of Polyolefin Microlayer Sheets", Composites Part B, **87**, 21–26 (2016), DOI:10.1016/j.compositesb.2015.09.052
- Tanner, R. I., "From A to (BK)Z in Constitutive Relations", J. Rheol., 32, 673–702 (1988), DOI:10.1122/1.549986

- Wagner, M. H., "Analysis of Time-Dependent Non-Linear Stress-Growth Data for Shear and Elongational Flow of a Low-Density Branched Polyethylene Melt", Rheol. Acta, **15**, 136–142 (1976), DOI:10.1007/BF01517505
- Wu, H., Zhao, G., Wang, G., Zhang, W. and Li, Y., "A New Core-Back Foam Injection Molding Method with Chemical Blowing Agents", Mater. Des., 144, 331–342 (2018), DOI:10.1016/j.matdes.2018.02.043
- Yu, M., Zhu, P. and Ma, Y., "Experimental Study and Numerical Prediction of Tensile Strength Properties and Failure Modes of Hollow Spheres Filled Syntactic Foams", Comput. Mater. Sci., 63, 232–243 (2012), DOI:10.1016/j.commatsci.2012.06.024
- Yu, M., Zhu, P. and Ma, Y., "Effects of Particle Clustering on the Tensile Properties and Failure Mechanisms of Hollow Spheres Filled Syntactic Foams: A Numerical Investigation by Microstructure Based Modeling", Mater. Des., 47, 80–89 (2013), DOI:10.1016/j.matdes.2012.12.004
- Yusa, A., Yamamoto, S., Goto, H., Uezono, H., Asaoka, F., Wang, L., Ando, M., Ishihara, S. and Ohshima, M., "A New Microcellular Foam Injection-Molding Technology Using Non-Supercritical Fluid Physical Blowing Agents", Polym. Eng. Sci., 57, 105–113 (2017), DOI:10.1002/pen.24391
- Zhu, Z., Park, C. B. and Zong, J. H., "Challenges to the Formation of Nano-cells in Foaming Processes", Int. Polym. Proc. 23, 270–276 (2007), DOI:10.3139/217.2050

Acknowledgements

Anish Kumar's Ph. D. Fellowship was funded through a Collaborative Project between CIPET and SABIC Technology and Research Private Ltd. Kishan Gurram, J. Rasia, and Anantharaman Dhanabalan are acknowledged for facilitating the collaborative effort. This work was carried out by Anish Kumar during an on-site project at SABIC Technology Center Bangalore, India. The authors acknowledge informative discussions with, and detailed review of this work by, Martin van Es; discussions with Leon Nelissen, Ed van de Gaar, Ton Sevriens, and Emanuel van der Ven from the SABIC Foam Technology Segment are also acknowledged. The authors acknowledge the IPP reviewers of the manuscript for suggesting several important changes and additions.

Date received: January 27, 2019 Date accepted: June 13, 2019

Bibliography DOI 10.3139/217.3801 Intern. Polymer Processing XXXIV (2019) 5; page 513–531 © Carl Hanser Verlag GmbH & Co. KG ISSN 0930-777X

Appendix

Al Material Model for the Matrix Portion of the Foam RVE – Rheological model for the Unfoamed Melt

For assigning to the matrix material, the rheological data for a widely characterized LDPE grade – studied in detail rheologically by Meissner (1971), and constitutively parameterized by Wagner (1976) and Chang and Lodge (1972) was chosen. The extensional viscosity measurements of this LDPE melt, reproduced in Fig. A1-1, display significant strain hardening which is ideal for producing high quality foams. The relaxation spectrum of the melt, which represents the linear stress-relaxation behavior using a Prony series (cf. Eqs. 1 and 2), as evaluated by Wagner (1976), is listed in Table A1-1.

$$G(t) = \sum_{i=1}^{N} a_i \lambda_i e^{\left(-\frac{t}{\lambda_i}\right)}, \tag{A1}$$

Relaxation Moduli =
$$g_i = a_i \lambda_i$$
. (A2)

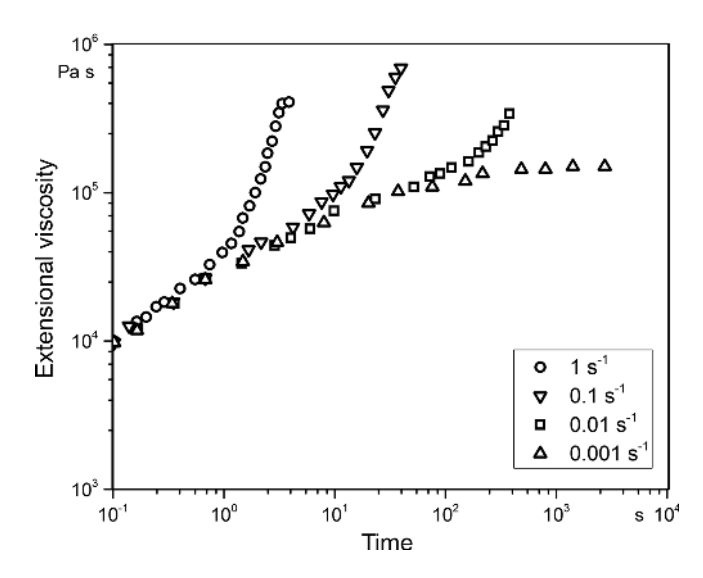


Fig. A1-1. Extensional viscosity as a function of time at different strain rates for the low-density branched polyethylene melt at 150°C. Data points read out from Fig. 1 of Wagner (1976), reporting the measurement of Meissner (1971)

| i | λ_i s | a _i dyne/cm ² s | g _i Pa |
|---|---------------|--|----------------------|
| 1 | 100 | 19.03 | 190.3 |
| 2 | 10 | 2 306 | 2306 |
| 3 | 1 | 62 410 | 6241 |
| 4 | 0.1 | 3 299 000 | 32990 |
| 5 | 0.01 | 37 200 000 | 37200 |

Table A1-1. Relaxation spectrum of LDPE, as characterized by Meissner (1971) and parameterized by Wagner (1976). This relaxation spectrum was assigned to the matrix phase of the foam RVE to obtain the stress-strain characteristics of the foam

As mentioned before, the first step in generation of a homogenized K-BKZ material model for the foam involved the constitutive parameterization of the matrix behavior. The choice of constitutive model for the matrix was governed by the choice of software where the tensile deformation of the foam RVE could be carried out. Since the RVE was rendered in DIGI-MAT FE (Digimat FE 2017 Documentation, MSC Software Corporation) and its interface with ABAQUS is established, it was decided to choose ABAQUS as the solver for solving of the foam RVE tensile deformation.

Therefore, the material models available to represent the matrix polymeric melt in ABAQUS were surveyed. Of course, ABAOUS (Analysis User's Guide, version 2016 and Theory Guide, version 2016, Dessault Systems) does not offer a fully nonlinear viscoelastic constitutive model in its library, which is required to accurately model a polymeric melt. The next option was a hyperelastic model. A hyperelastic model can simulate incompressibility and tensile strain hardening, both of which are critical characteristics of a polymeric melt undergoing tensile deformation macroscopically during blowing, and microscopically in the bridges between the foam cells. The hyperelastic model may also be ideally combined with a viscoelastic Prony series (ABAQUS, Theory Guide, version 2016, Dessault Systems) to arrive at a Lodge-rubber like behavior (Christopher, 1994) that can simulate both strain hardening and strain rate dependence. However, in order to keep the demonstration of the framework relatively simple, only the key phenomenon associated with morphology evolution, namely the ability to account for strain-dependent effects was incorporated in the simulation. Therefore, only a hyperelastic model (without rate dependent effects) was chosen to represent the matrix for the RVE simulation in ABAQUS.

The constitutive behavior of isotropic hyperelastic material is defined by the equation relating the strain energy function (SEF) 'W' based on the three invariants of the strain tensor (Bower, 2010).

$$W = f(I_1, I_2, I_3). (A3)$$

 I_1 , I_2 , and I_3 , are the invariants of the Green deformation tensor, and defined in terms of the principal stretch ratios λ_1 , λ_2 , and λ_3 (Shahzad et al., 2015):

$$I_1 = \lambda_1^2 + \lambda_2^2 + \lambda_3^2, \tag{A4}$$

$$I_2 = \lambda_1^2 \lambda_2^2 + \lambda_2^2 \lambda_3^2 + \lambda_3^2 \lambda_1^2, \tag{A5}$$

$$I_3 = \lambda_1^2 \lambda_2^2 \lambda_3^2. \tag{A6}$$

The third invariant of the tensor $I_3 = 1$ as the hyperelastic material is considered to be incompressible. Therefore, the SEF is function of I_1 , and I_2 i.e.

$$W = f(I_1 - 3, I_2 - 3). (A7)$$

Out of the several SEF forms available in ABAQUS, such as the Reduced Polynomial, Ogden, Yeoh, Arruda-Boyce, Marlow, and Van der Waals (ABAQUS, Analysis User's Guide, version 2016, Dessault Systems), the Ogden form, shown in Equation A8, was chosen to fit the experimental data.

$$W = \sum_{i=1}^{N} \frac{2\mu_i}{\alpha_i^2} \left(\lambda_1^{\alpha_i} + \lambda_2^{\alpha_i} + \lambda_3^{\alpha_i} - 3\right) + \sum_{i=1}^{N} \frac{1}{D_i} \left(J^{el} - 1\right)^{2i}, \tag{A8} \label{eq:A8}$$

N is the number of modes (max N = 6 is available in ABAQUS (Analysis User's Guide, version 2016, Dessault Systems)), and μ_i and α_i are material constants.

The parameterization of the matrix rheology then requires the identification of the value of N, and the determination of μ_i and α_i associated with the Ogden model that best fits the highstrain melt behavior shown in Fig. A1-1. Out of the extensional viscosity curves available from the experiments of Meissner (1971) at several strain rates, the curve at the highest strain rate of 1 s⁻¹ was chosen to be parameterized using the hyperelastic model. The data at the highest available strain rate was chosen since during blow molding large deformations are affected in short times of the order of a few seconds, resulting in high strain rates. The extensional viscosity (η_E) vs. time curve available from Meissner (cf. Figure A1-1) was first converted to an engineering stress vs. engineering strain curve. The extensional viscosity was multiplied by the constant strain rate (έ) of 1 s⁻¹ to get the engineering stress (σ) of the melt. The experimental time was multiplied again by the constant strain rate of 1 s⁻¹ to get the true strain (e) during extension of the melt. The true strain was then converted to engineering strain (E) using the formula shown in equations below.

$$\tau = \eta_E \dot{\epsilon}, \tag{A9}$$

$$e = t\dot{\epsilon},$$
 (A10)

$$\varepsilon = \exp(e) - 1. \tag{A11}$$

The engineering stress-strain curve was then fed into the "ABAQUS \rightarrow Material \rightarrow Evaluate" function (ABAQUS, Analysis User's Guide, version 2016, Dessault Systems) and Ogden models with multiple modes were evaluated for fit with the experimental data as well as stability. Out of the various orders of Ogden models evaluated, the model with N = 3 displayed adequate fit and the best stability among all the models at all strains and loading scenarios as evaluated by ABAQUS using a single element simulation. The predicted Ogden N = 3 model parameters were then fed into a finite element simulation of a rectangular multi-element block to represent the uniaxial tensile deformation of the matrix. The results from these simulations are compared with experimental data in Fig. 4 within Section 3.1.3.

A2 Considerations in Creation of Foam Representative Volume Element

Figure A2-1A shows a typical representative volume element (RVE) (Bardella et al., 2012; Cho et al., 2017; Marur, 2010; Yu et al., 2012, 2013) for a foam generated using DIGIMAT-FE (Digimat FE 2016, Computer Software, MSC Software Corporation). It may be observed from Fig. A2-1 that the voids generated in DIGIMAT are randomly distributed in the 3D bounding space and satisfy 3D periodicity. Certain idealization assumptions have been made while generating the RVE, which are: (i) all the voids are of spherical shape and (ii) there is no interpenetration between voids (i. e., no coalescence). The matrix (void-free or solid) portions of the RVE were modelled using the 3-mode Ogden hyperelastic model representing the unfoamed melt, described in Appendix A1 (the Ogden parameters listed in Table 1).

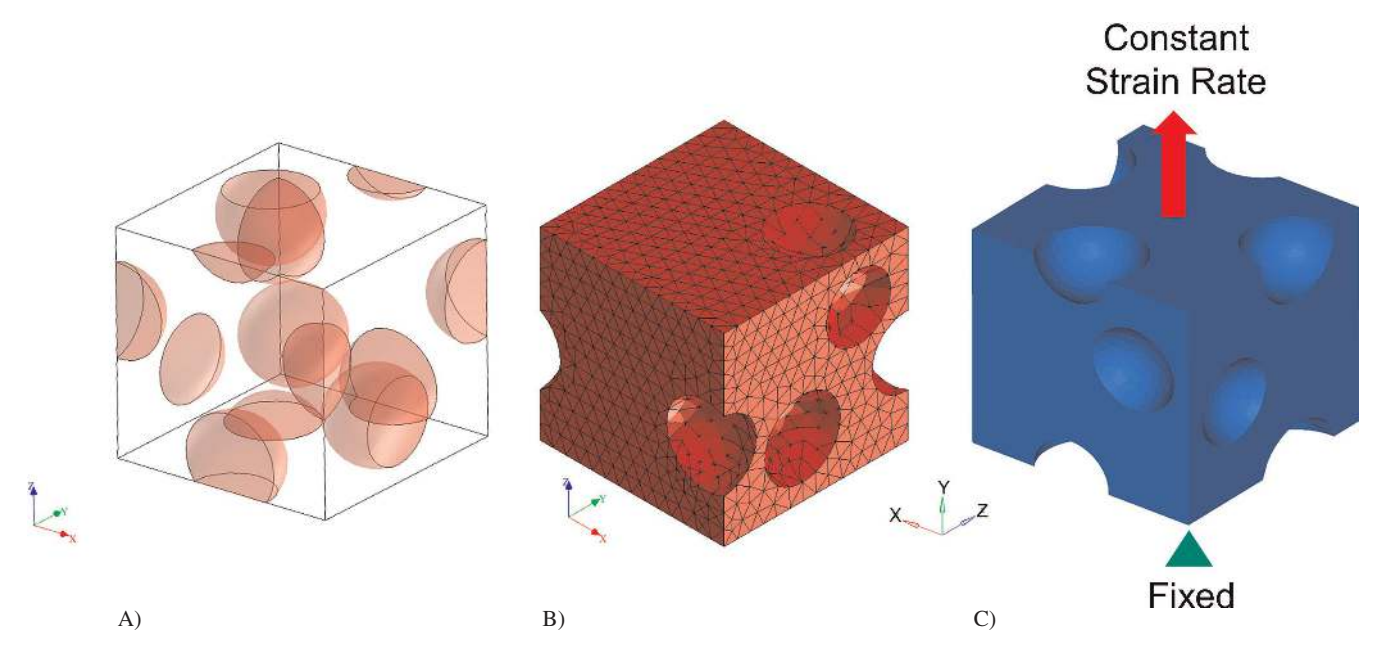


Fig. A2-1. Representative Volume Element (RVE) of the foam generated using the parameters provided in Table 1 (A), and employed in simulations for generation of the uniaxial deformation characteristics of the foam, and (B) discretization of the foam RVE using a conformal mesh generated in DIGIMAT and (C) the boundary conditions imposed on the foam RVE to simulate uniaxial extensional deformation

In generating an RVE for representing a foam with a chosen cell volume fraction, several parameters may be varied. These are the RVE size, the cell size, the cell size distribution, and the stochasticity or randomness associated with the generation of the RVE with a given set of parameters.

Before choosing an RVE to generate the stress-strain curve for the foam, a parametric study was systematically carried out to evaluate whether the aforementioned parameters associated with the RVE have any influence on the predictions. In order to carry out the parametric study, each RVE generated with a chosen set of parameters, was first meshed using an algorithm available in DIGIMAT to obtain a conforming mesh using C3D10H hybrid tetrahedral elements as shown in Fig. A2-1B (DIGIMAT does not allow voxel mesh for voids) (Digimat FE, 2017 Documentation, MSC Software Corporation). This RVE was then subjected to a tensile deformation simulation to get the stress-strain response.

As shown in Fig. A2-1C, the boundary condition for a constant strain rate uniaxial extension was imposed on the top face of the RVE. It needs to be noted that the "true" strain rate was kept constant in the simulation, which means that the length of the specimen increases exponentially over time unlike in a

conventional tensile test experiment where the length increases linearly with time resulting in a constant "engineering" strain rate. This boundary condition was imposed to mimic the typical uniaxial extensional viscosity measurement experiment that is performed on melts at constant Hencky (or logarithmic) strain rates. Also, the kinematics of a constant Hencky strain rate extension are easier to implement with the K-BKZ model. Since the simulated stress-strain curve form the RVE simulation would have to be analysed using K-BKZ model for its parameterization, it would be essential to have kinematics that are easy to integrate using the K-BKZ integral equation.

For the uniaxial tensile simulation of the RVE, the default periodic boundary conditions were imposed on the side walls imposing continuity on both X-Y and Y-Z planes. Also, one of the bottom corners of the RVE was fixed for stability purposes. The uniaxial tensile simulation was carried out up to a true strain of 3.0 (300%). Using the above steps, parametric studies were carried out to systematically assess (1) the effect of stochasticity or randomness in placement of cells in the RVE (Fig. A2-2); (2) the effect of cell size, number density and RVE size (as shown in Fig. A2-3); and (3) the effect of cell-size distribution (Fig. A2-4), on the predicted foam char-

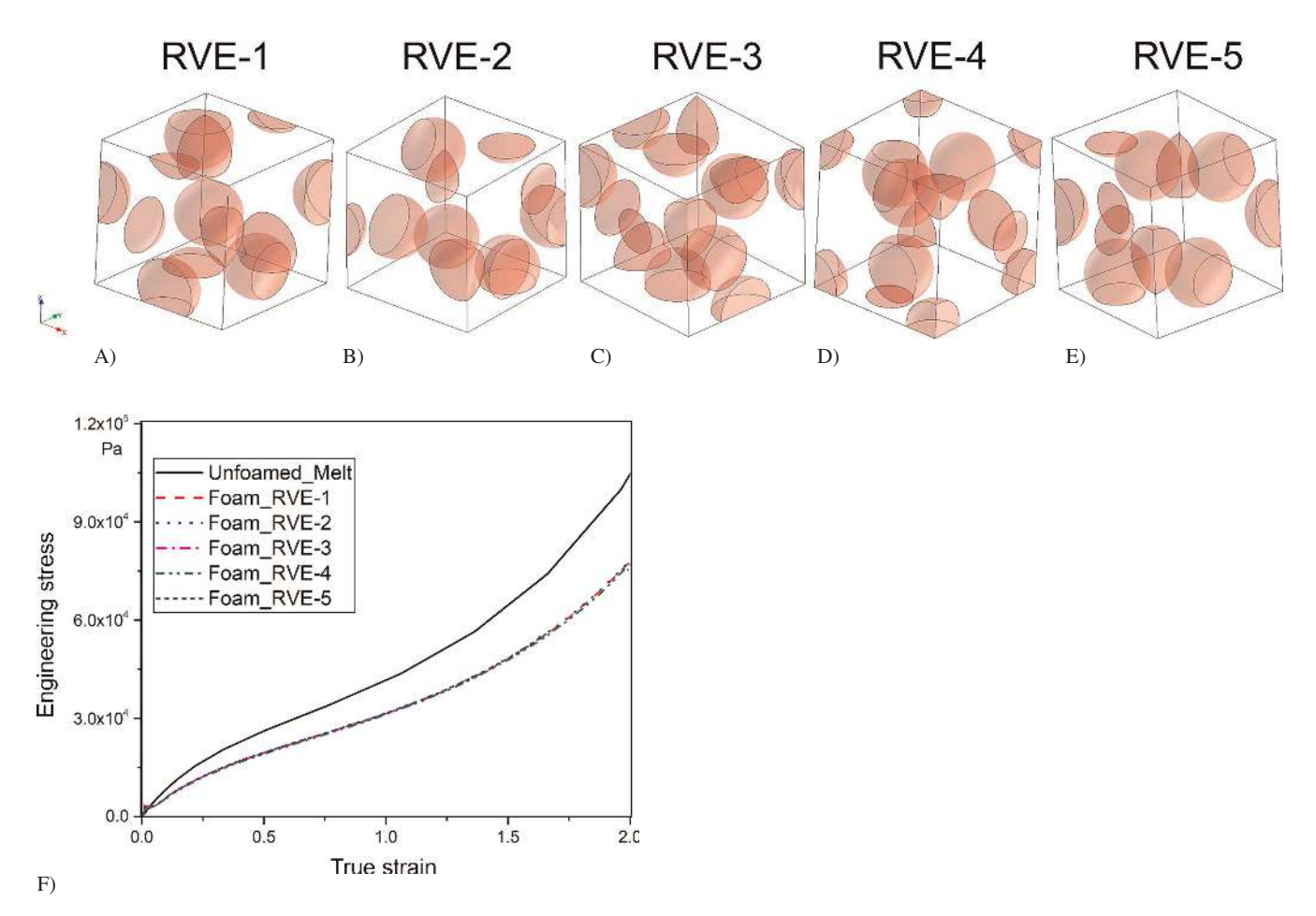


Fig. A2-2. RVE calibration – effect of randomness: A to E) five versions of randomly generated foam representative volume elements (RVEs) using the same set of parameters: void or cell volume fraction 0.2; number of cells 5; total RVE volume 1 mm^3 ; uniform (monodisperse) cell diameter 0.42 mm; and F) the simulated uniaxial tensile stress-strain curve of the foam for these five versions (with the matrix property simulated using the Ogden model with parameters shown in Table 1 in the main text)

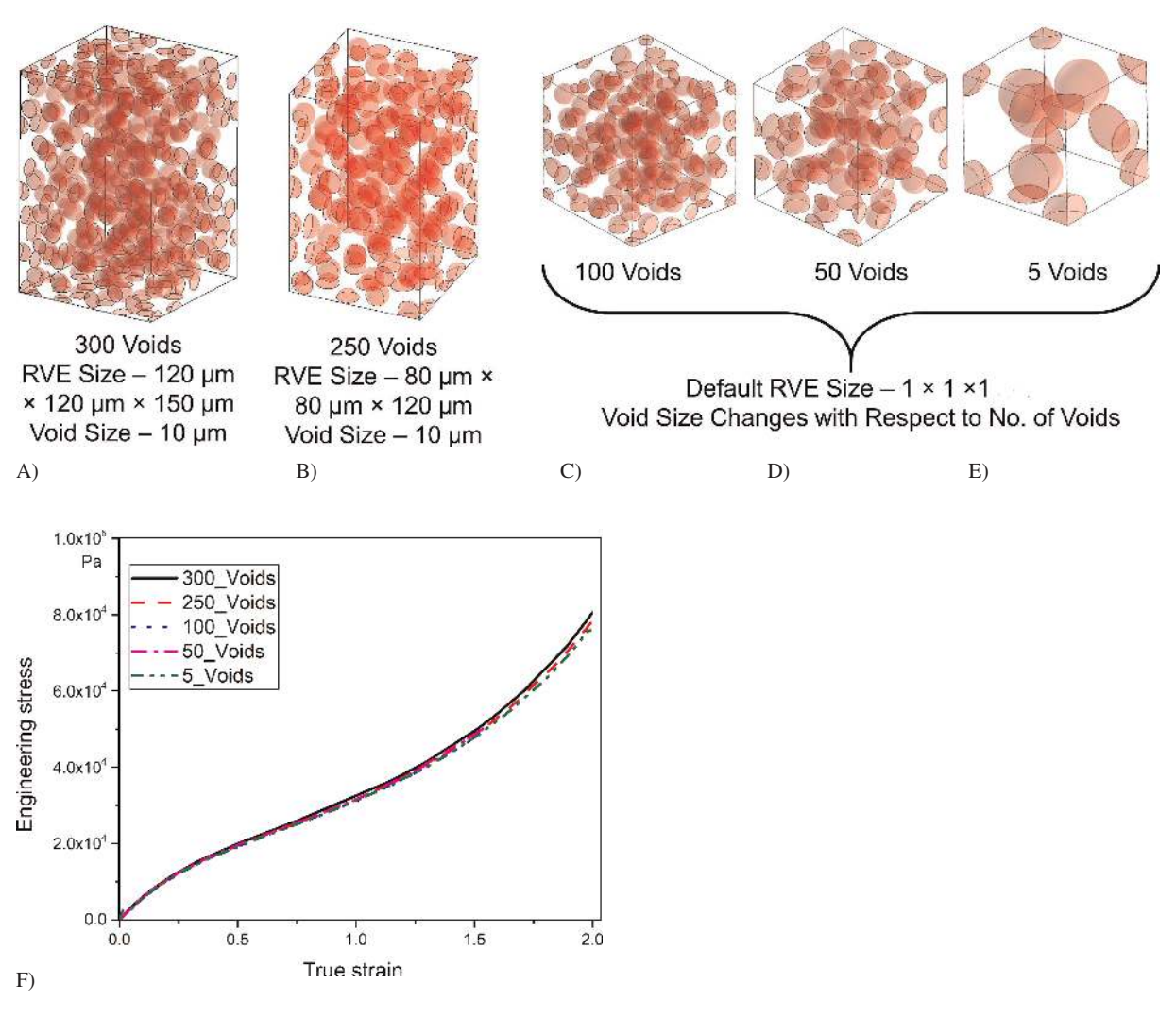


Fig. A2-3. RVE calibration – effect of cell size, number density and RVE size: A to E) five versions of foam RVEs with cell volume fraction 0.2, and generated with different settings of cell size, number of cells with corresponding changes in RVE volume; and (F) the simulated uniaxial tensile stress-strain curve of the foam for these three versions (with the matrix property simulated using the Ogden model with parameters shown in Table 1)

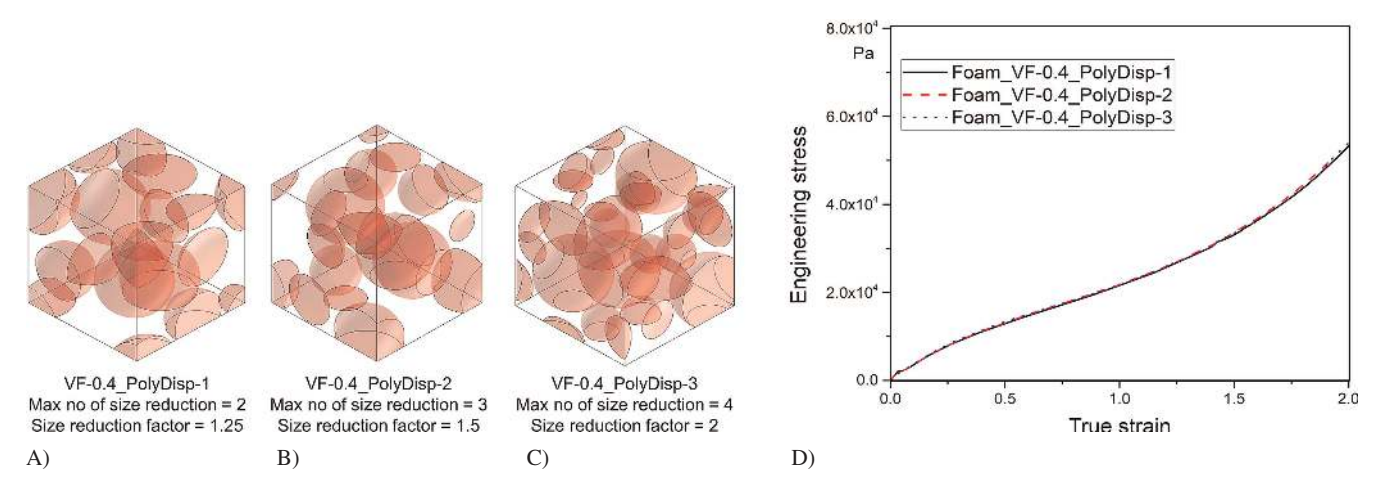


Fig. A2-4. RVE calibration – effect of cell size distribution: A to C) three versions of foam RVEs with void or cell volume fraction 0.4, and generated with different cell size distributions; D) the simulated uniaxial tensile stress-strain curve of the foam for these three versions (with the matrix property simulated using the Ogden model with parameters shown in Table 1)

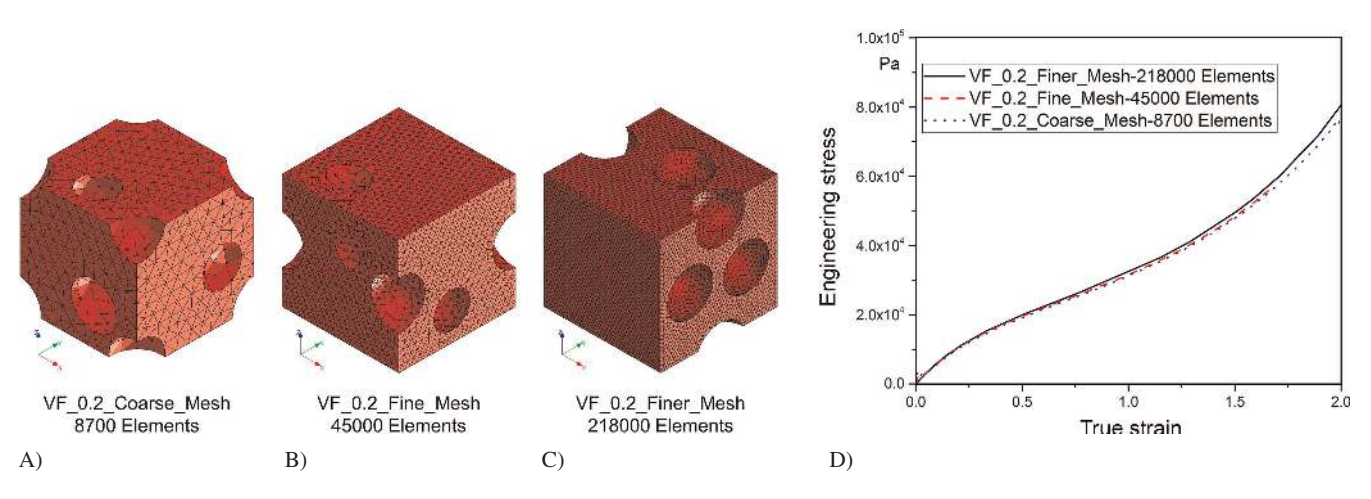


Fig. A2-5. RVE calibration – grid independence studies: Foam RVE with void or cell volume fraction 0.2; number of cells 5; total RVE volume 1 micro-m³; uniform cell diameter 0.42 micro-m, discretized using coarse (A), default (B), finer tetrahedral mesh elements (C) and (D) the simulated uniaxial tensile stress-strain curve of the foam for these three versions (with the matrix property simulated using the Ogden model with parameters shown in Table 1)

acteristics. Further, a grid independence study was also carried out to arrive at the best combination of accuracy and computational efficiency in the RVE simulations (Fig. A2-5). From inspection of Figs. A2-2 to A2-4, it is clear that for a fixed vol-

ume fraction, the parameter settings for cell size, cell number, cell-size-distribution, and RVE size, as well as the randomness in cell placement do not have an impact on the predicted stress-strain response of the RVE.